Proceedings of DETC'00
2000 ASME Design Engineering Technical Conferences
September 10-14, 2000, Baltimore, Maryland, USA

DETC00/MECH-14116

MODELING AND BATCH FABRICATION OF SPATIAL MICRO-MANIPULATORS

C. Kimball
Department of Mechanical Engineering and
Institute for Systems Research
University of Maryland
College Park, Maryland 20742
Email: ckimball@isr.umd.edu

L.W. Tsai
Department of Mechanical Engineering and
Institute for Systems Research
University of Maryland
College Park, Maryland 20742
Email: lwtsai@isr.umd.edu

D. DeVoe
Department of Mechanical Engineering and
Institute for Systems Research
University of Maryland
College Park, Maryland 20742
Email: ddev@eng.umd.edu

J. Maloney
Department of Mechanical Engineering and
Institute for Systems Research
University of Maryland
College Park, Maryland 20742
Email: maloneyj@glue.umd.edu

ABSTRACT

Pseudo rigid body models(PRBM) may be used to accurately and efficiently model the large elastic deflections of compliant mechanisms. Previously published models have only considered end forces with no end moment or end moment acting only in the same direction as the force. In this paper, we present a model for a cantilever beam with end moment acting in the opposite direction as the end force causing an inflection point. As motivation for the development of such models, we present a novel spatial micro-manipulator which can be modeled with this PRBM. This micro-manipulator is being fabricated as a MEMS device using a 3D fabrication process.

INTRODUCTION

In this paper, we present an improved method of modeling compliant mechanisms, and as motivation for such models, discuss the modeling and fabrication of a compliant spatial micro-manipulator. Micro-spatial manipulators differ significantly from their traditional counterparts in the types of joints which can be used. While it is possible to make a true revolute joint in a planar MEMS device, it is not practical in a spatial micro-manipulator. Therefore, flexural sections must be used instead of traditional joints. To analyze and control the motion of such a mechanism, it is desirable to have a simplified model of the flexural sections. This can be accomplished by modeling the response of an individual flexural section fixed at one end with loads applied to the free end. This model can then be applied to each of the flexural sections in a compliant manipulator. Such models have been developed for cases in which only force is applied to the free end (Howell, 1995) and moment acts in the same direction as the end force (such a moment is considered positive) (Saxena, 1998). These models have been applied to mechanisms for which end moments in the compliant sections can be assumed to be zero or positive, such as in parallel-guiding mechanisms (Derderian, et al., 1996). In the manipulator shown in Figure 1, it is clear that end moments will be present in some of the compliant sections, and may act in the opposite direction as the force, possibly creating an inflection point. Therefore, we have developed a model for a flexural section with end moment acting in the opposite direction as the end force creating an inflection point.

We wish to fabricate 3-D spatial micro-manipulators in a parallel process (simultaneously fabricating many individual structures on a single silicon wafer). There are a

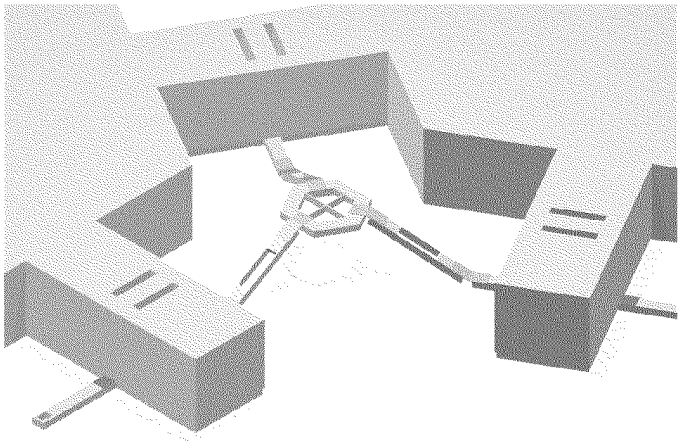

Figure 1. 3 DOF spatial micro-manipulator being fabricated. The manipulator has purely translational motion.

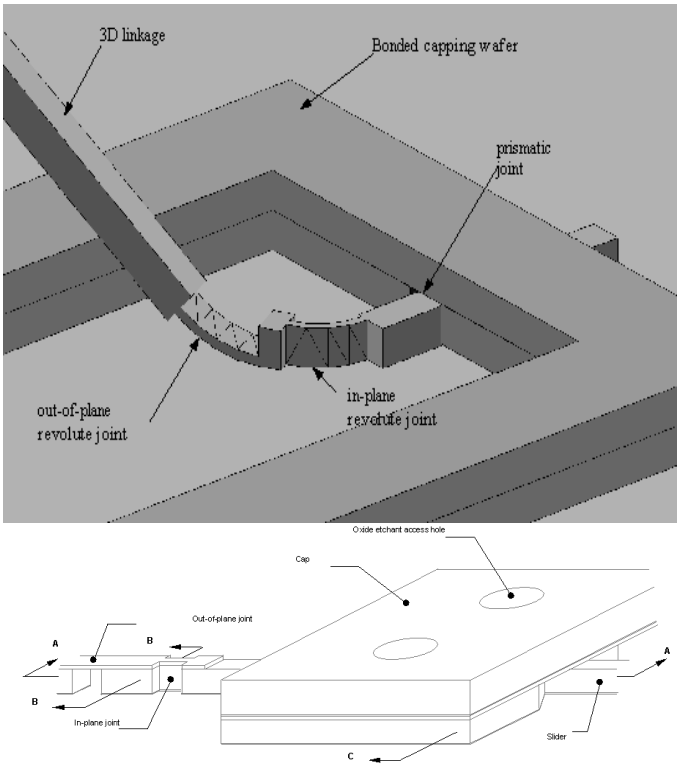

Figure 2. View of in-plane and out-of-plane joints which allow a manipulator manufactured in a planar configuration to possess spatial motion.

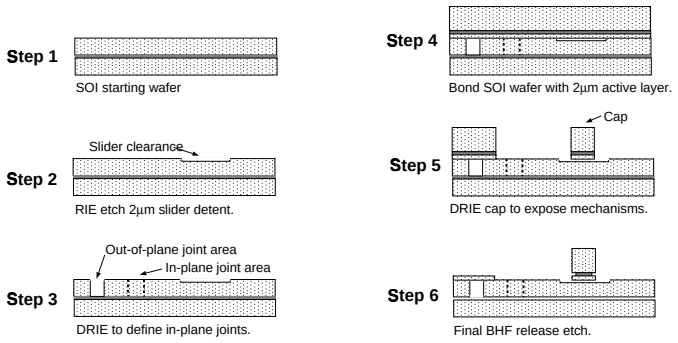

Figure 3. Process flow for 3DMEMS planar process. The cross-section shown is cut A-A shown in Fig. 2

.

variety of micro-fabrication techniques available for producing 3-D structures. However, not all techniques are capable of producing spatial micro-manipulators, and not all 3-D processes can be done in parallel. Processes such as LIGA, Deep Reactive Ion Etching (DRIE), and laser etching are only capable of producing extrusions of two dimensional patterns. Some processes capable of producing 3-D spatial manipulators, such as micro stereo lithography and focused laser/ion beam deposition, are serial processes (structures on the wafer must be made one by one, greatly increasing the time and cost of fabrication). Other processes, such as component bonding and hinged structure fabrication, require manual assembly, making them poorly suited for low cost, mass fabrication. Therefore, we are developing a 3-D parallel fabrication process using DRIE to etch wafers which are then bonded together. This process is capable of producing overhangs and enclosed components, both of which are necessary for spatial manipulators.

DESIGN OF 3 DOF SPATIAL MICRO-MANIPULATOR

A MEMS spatial manipulator may be fabricated in two ways. The manipulator may be made in a vertical configuration, which requires patterning and bonding many layers together. Alternatively, the manipulator may be made in a planar (singular) configuration using only two wafers. After fabrication, the manipulator is moved out of the plane and away from its singular configuration. The 3 DOF spatial micro-manipulator, shown in Fig. 1, is manufactured using the latter method. It is shown in Fig 1 after moving away from its initial position. The manipulator has three limbs, each limb containing a base connected slider used for actuation and four compliant sections used to approximate revolute joints. The mechanism is based on a macro-scale 3 DOF parallel manipulator possessing only translational degrees of freedom (Tsai and Stamper, 1996). The manipulator investigated in (Tsai and Stamper, 1996) employs base connected revolute joints which are actuated by mo-

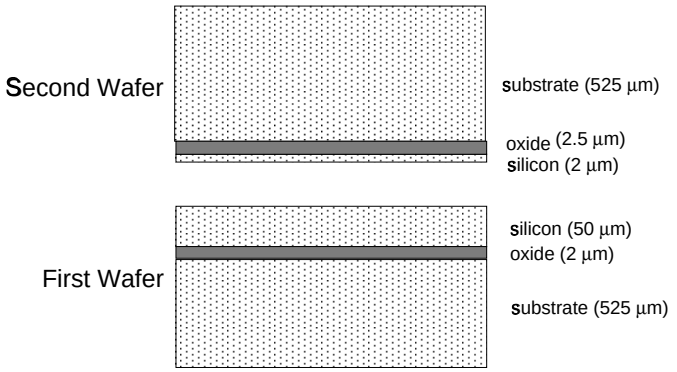

Figure 4. Layer names for 3DMEMS planar process.

tors. However, linear displacement is the easiest form of actuation for MEMS devices, so the base-connected revolute joints are replaced by base-connected prismatic joints (sliders). In addition, the four bar mechanism in each limb of (Tsai and Stamper, 1996) is replaced by two parallel compliant sections. Using a parallel manipulator allows multiple degrees of freedom (DOF) to be achieved while all actuators remain on the base. In contrast, a multi-DOF serial manipulator would require some form of actuation at the intermediate joints. The use of a parallel manipulator also increases the external load capacity of the output, since external loads are shared by multiple limbs.

The fabrication steps are shown in Fig. 3, which shows a vertical cross-sectional cut taken along the length of one of the limbs (cut A-A of Fig. 2). The starting SOI wafer in step 1 is commercially available, but custom layer thicknesses can also be achieved by making the desired SOI wafer from scratch using oxide growth, chemical-mechanical polishing (CMP), and thermal bonding. In step 2, a clearance area for the slider is etched with reactive-ion etching (RIE). This prevents the top of the slider from bonding to the cap. Step 3 is a deep reactive-ion etch (DRIE) completely through the 50 μm layer of the first wafer, which defines the main features of the first wafer. The shape of the in-plane joint area is defined by the mask; the out-of-plane joint area is etched completely through. A 2 μm gap is etched between the slider and the guides to allow slider motion. The second wafer, which is used for both the out-of-plane joint and the slider cap, is bonded to the first in step 4. In step 5, the entire second wafer is etched completely away around the end of the slider via DRIE (right side of Fig. 3, step 5). Additionally, a gap is etched between the slider and the cap to allow slider motion. In the last step, a 75 μm timed oxide etch is performed to release the slider. It is necessary for the cap and guides to be much larger than 75 μm so that they remain anchored to the substrate of the first wafer. Alignment between wafers is achieved by pre-etching successively larger DRIE alignment holes in the periphery of each wafer, allowing direct topside optical alignment without the need for an IR alignment system or wafer-to-wafer alignment during the bonding process. This approach enables device fabrication without the need for costly, specialized alignment systems.

SOLUTIONS FOR LARGE DEFLECTIONS OF A CANTILEVER BEAM

To develop a model for the large deflection of a flexural section, the actual deflections are determined, and appropriate dimensions for a rigid body model are determined through optimization. The Bernoulli-Euler beam equation, which states that the moment at any point in a beam is proportional to its curvature at that point, can be used to solve large deflection problems. The Bernoulli-Euler equation can be written as

$$M = EI\frac{d\theta}{ds} = EI\frac{\frac{d^2y}{dx^2}}{(1+(\frac{dy}{dx})^2)^{3/2}} \qquad (1)$$

where M is the moment, $d\theta/ds$ is the rate of change of angular deflection along the beam, EI is the flexural rigidity of the beam, x is the distance along the undeflected beam axis, and y is the transverse deflection. For small deflections, dx/dy is small, and so $(dx/dy)^2$ can be neglected, leading to the standard linearized beam theory. However, in large deflections, such as the deflections seen in compliant mechanisms, this term is large and may not be neglected. In this case, Eq. (1) may be solved either through a classical method using elliptic integrals (Howell, 1995; Bisshop, 1945; Frisch-Fay, 1963; Mattiasson, 1981) or numerically (Saxena, 1998). The elliptic integral solutions are used here, as they provide a simple method of determining when an inflection point will occur.

Equation (1) can be rewritten as (see Howell, 1995 for derivation)

$$\frac{d\theta}{ds} = \pm\sqrt{2\frac{P}{EI}(-\sin\theta + n\cos\theta + \sin\theta_o - n\cos\theta_o) + \left(\frac{M_o}{EI}\right)^2} \qquad (2)$$

The loads P, nP, and M_o are shown in Fig. 5 (n is the ratio of horizontal to vertical force), and EI is the flexural rigidity of the beam. In the following discussion, P is assumed to be positive, and M_o is assumed to be negative. The arc length s is measured from the fixed end of the beam, and the angle $\theta(s)$ is measured from the x axis at a distance s along the beam. θ_o is the angle of the free end of the beam. The sign of $d\theta/ds$ is determined by θ_o and the loading

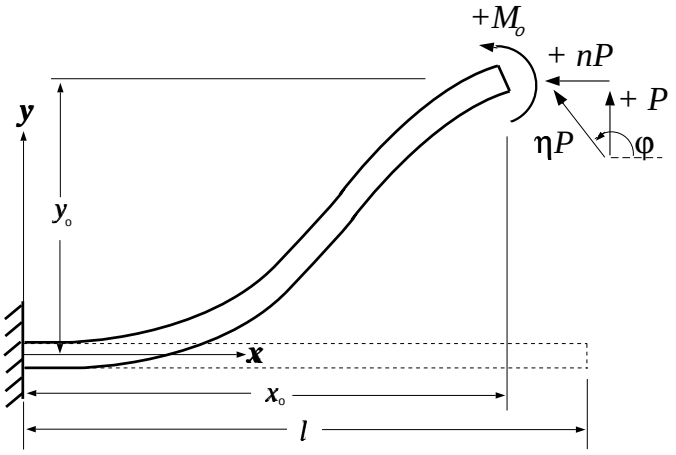

Figure 5. Beam with external bending moment, vertical force, and horizontal force causing an inflection point. n is the ratio of horizontal force to vertical force, and (x_o, y_o) is the position of the free end of the beam. In this work, M_o is always negative.

conditions. If no inflection point exists, then the slope is either monotonically increasing or decreasing, $d\theta/ds$ must always be positive or negative, respectively. In this case, the sign of $d\theta/ds$ is equal to the sign of θ_o. If an inflection point exists, then $d\theta/ds$ is positive before the inflection point and negative after. Separating variables, Eq. (2) can be written as

$$\frac{P}{EI}ds = \pm\frac{d\theta}{\sqrt{2(-\sin\theta + n\cos\theta + \sin\theta_o - n\cos\theta_o) + \frac{M_o^2}{PEI}}} \tag{3}$$

Defining the following non-dimensional constants,

$$\alpha = \sqrt{\frac{Pl^2}{EI}} \qquad \text{and} \qquad \kappa = \frac{1}{2}\frac{M_o^2}{PEI}, \tag{4}$$

Eq. (3) may be written as

$$\frac{\alpha}{l}ds = \pm\frac{d\theta}{\sqrt{2}\sqrt{-\sin\theta + n\cos\theta + \sin\theta_o - n\cos\theta_o + \kappa}}. \tag{5}$$

Integrating Eq. (5) and defining

$$\lambda = \sin\theta_o - n\cos\theta_o + \kappa \tag{6}$$

yields a relationship between the angle of the free end of the beam, θ_o, and the applied load α.

$$\alpha = \pm\frac{1}{\sqrt{2}}\int_0^{\theta_o}\frac{d\theta}{\sqrt{\lambda - \sin\theta + n\cos\theta}} \tag{7}$$

The plus or minus sign is chosen as described earlier: positive for monotonically increasing slope and negative for monotonically decreasing slope. This sign convention ensures that α is always positive (when θ_o is negative, the integral becomes negative, because the upper limit of integration is less than the lower). This is consistent with the definition of α given in Eq. (4), where α is a square root which must always be positive.

To find the x and y displacements of the beam tip, $d\theta/ds$ can be rewritten as:

$$\begin{aligned}\frac{d\theta}{ds} &= \frac{d\theta}{dx}\frac{dx}{ds} = \frac{d\theta}{dx}\cos\theta \\ \frac{d\theta}{ds} &= \frac{d\theta}{dy}\frac{dy}{ds} = \frac{d\theta}{dy}\sin\theta\end{aligned} \tag{8}$$

Using Eqs. (8) and (6), Eq. (5) can be written as (Howell, 1995)

$$\frac{x_o}{l} = \pm\frac{1}{\alpha\sqrt{2}}\int_0^{\theta_o}\frac{\cos\theta\, d\theta}{\sqrt{\lambda - \sin\theta + n\cos\theta}} \tag{9}$$

$$\frac{y_o}{l} = \pm\frac{1}{\alpha\sqrt{2}}\int_0^{\theta_o}\frac{\sin\theta\, d\theta}{\sqrt{\lambda - \sin\theta + n\cos\theta}} \tag{10}$$

where (x_o, y_o) represent the deflected position of the free end of the beam, as shown in Fig. 5. Equations (7), (9), and (10) are functions of $\theta(s)$. If no inflection point exists, then $\theta(s)$ is either a monotonically increasing or monotonically decreasing single-valued function. However, if an inflection point exists, then $\theta(s)$ becomes a multi-valued function. $\theta(s)$ increases from zero to θ_i, and then decreases from θ_i to θ_o, where θ_i is always greater than θ_o. In this case, the integrals must be split into two parts. $d\theta/ds$ is positive from the fixed end until the inflection point, where $d\theta/ds = 0$. After the inflection point, $d\theta/ds$ is negative. Therefore, in the first integral, the positive signs of Eqs. (7), (9), and (10) are taken, whereas for the second integral, the negative signs are taken.

$$\alpha = \frac{1}{\sqrt{2}}\left(\int_0^{\theta_i}\frac{d\theta}{\sqrt{\lambda - \sin\theta + n\cos\theta}} + \int_{\theta_o}^{\theta_i}\frac{d\theta}{\sqrt{\lambda - \sin\theta + n\cos\theta}}\right) \tag{11}$$

$$\frac{x_o}{l} = \frac{1}{\alpha\sqrt{2}}\left(\int_0^{\theta_i}\frac{\cos\theta\, d\theta}{\sqrt{\lambda - \sin\theta + n\cos\theta}} +\right.$$

$$\int_{\theta_o}^{\theta_i} \frac{\cos\theta\, d\theta}{\sqrt{\lambda - \sin\theta + n\cos\theta}}\Bigg) \tag{12}$$

$$\frac{y_o}{l} = \frac{1}{\alpha\sqrt{2}}\Bigg(\int_0^{\theta_i} \frac{\sin\theta\, d\theta}{\sqrt{\lambda - \sin\theta + n\cos\theta}} + \int_{\theta_o}^{\theta_i} \frac{\sin\theta\, d\theta}{\sqrt{\lambda - \sin\theta + n\cos\theta}}\Bigg) \tag{13}$$

These equations can be solved using Jacobi's elliptic integrals of the first and second kind, denoted by $F(\gamma, k)$ and $E(\gamma, k)$, respectively.

$$F(\gamma,k) = \int_0^{\gamma} \frac{d\theta}{\sqrt{1 - k\sin^2\theta}}, \quad E(\gamma,k) = \int_0^{\gamma} \sqrt{1 - ksin^2\theta}d\theta \tag{14}$$

The complete elliptic integrals of the first and second kind are defined to be

$$F(k) = F(\frac{\pi}{2}, k), \qquad E(k) = E(\frac{\pi}{2}, k) \tag{15}$$

Using Eqs. (14) and (15), Eqs. (11), (12), and (13) can be written as (Byrd, 1954)

$$\alpha = \frac{1}{\sqrt{\eta}} f_F(\gamma_1, \gamma_2, k) \tag{16}$$

$$\frac{x_o}{l} = \frac{1}{\alpha\eta^{5/2}}\Big(-n\eta\,(f_F(\gamma_1,\gamma_2,k) - 2f_E(\gamma_1,\gamma_2,k)) + \sqrt{2\eta(\eta+\lambda)}(\cos\gamma_1 + \cos\gamma_2)\Big) \tag{17}$$

$$\frac{y_o}{l} = \frac{1}{\alpha\eta^{5/2}}\Big(\eta\,(f_F(\gamma_1,\gamma_2,k) - 2f_E(\gamma_1,\gamma_2,k)) + n\sqrt{2\eta(\eta+\lambda)}(\cos\gamma_1 + \cos\gamma_2)\Big) \tag{18}$$

where

$$f_F(\gamma_1,\gamma_2,k) = 2F(k) - F(\gamma_1,k) - F(\gamma_2,k) \tag{19}$$

$$f_E(\gamma_1,\gamma_2,k) = 2E(k) - E(\gamma_1,k) - E(\gamma_2,k) \tag{20}$$

$$\eta = \sqrt{1+n^2} \tag{21}$$

$$k = \frac{\eta+\lambda}{2\eta} \tag{22}$$

$$\gamma_1 = \sin^{-1}\left(\sqrt{\frac{\eta-n}{\eta+\lambda}}\right) \tag{23}$$

$$\gamma_2 = \sin^{-1}\left(\sqrt{\frac{\eta - n\cos\theta_o + \sin\theta_o}{\eta+\lambda}}\right) \tag{24}$$

Equations (16)-(18) parameterize the deflection of the free end of the beam as a function of the end angle, θ_o, for loading conditions which produce an inflection point. The loading conditions are defined by the non-dimensional parameters κ, n (which are ratios of applied moment/applied force, and horizontal force/vertical force, respectively), and α (which measures the magnitude of the loads). Given the three load parameters, Eq. (16) must be solved numerically for θ_o, which is then used in Eqs. (17) and (18). However, if the equations are restricted to a range of θ_o over which $\alpha(\theta_o)$ is a bijective mapping, then θ_o can be used as a load parameter instead of α. An inflection point exists when the following relationships are satisfied:

$$\eta - |\kappa + \sin\theta_o - n\cos\theta_o| > 0 \tag{25}$$

$$n + \kappa + \sin\theta_o - n\cos\theta_o \geq 0 \tag{26}$$

$$\phi - \pi \leq \theta_o \leq \phi \tag{27}$$

$$\kappa > 0 \tag{28}$$

where

$$\phi = tan^{-1}\frac{1}{-n} \tag{29}$$

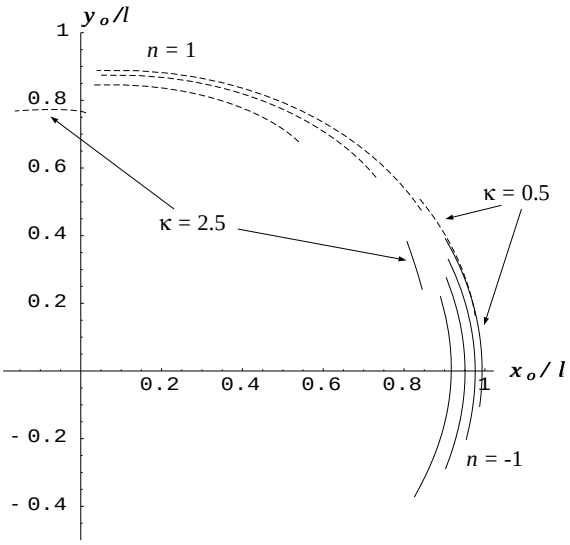

Figure 6. Deflection paths of the free end of the beam for loading conditions which produce an inflection point. The dashed lines represent $n = 1$, and the solid line represents $n = -1$. As n increases, the deflections increase. As κ increases, the deflection paths are shorter, closer to the origin, and resemble straight lines.

Equations (25)-(28) come from the elliptic integral solution (Byrd, 1954). The following constraint for compliant mechanisms is also imposed on the deflection equations.

$$-\frac{\pi}{4} \leq \theta_o \leq \frac{\pi}{4} \tag{30}$$

Since a compliant mechanism will not usually be deflected more than 45°, and modeling larger deflections becomes more complicated, the pseudo rigid body model is limited to ±45°.

METHOD OF OPTIMIZATION TO DETERMINE PRBM

Given a set of non-dimensional loads κ, n, and α (or κ, n, and θ_o), Eqs. (25) - (28) can be used to determine if an inflection point exists, and if so, Eqs. (17) and (18) can be used to determine the deflection of the beam free end. For any fixed values of κ and n, sufficiently small values of α do not produce an inflection point. Physically, this is due to the non-dimensional parameterization given in Eq. (4), which can be re-written as $M_o = \sqrt{2EI\kappa}\sqrt{P}$. When $P \ll 1$, then $M_o \propto \sqrt{P} > P$ and so moment dominates, and the beam deflects in the negative y direction ($\theta_o < 0$) without an inflection point. This solution is described by a different set of elliptic integral equations. When P becomes sufficiently large, the effect of the force becomes more significant and an inflection point will exist. Finally, there is a maximum value of P (or equivalently α, or equivalently θ_o) beyond which the elliptic integral solution is no longer valid. Figure 6 shows how κ and n affect the path traced by the free end of the beam. For low values of κ (regardless of n), the path of the beam tip is close to a circular arc, closely resembling the load cases investigated previously (Howell, 1995) and (Saxena, 1998). When the deflection path is a circular arc, a model with one revolute joint and an angle correction at the free end may be used, as in (Howell, 1995) and (Saxena, 1998). However, for large values of κ, the path is closer to a straight line than a circular arc. Therefore, a model with one pivot point is not adequate for a beam with an inflection point. This suggests using a model with two pivot points, as shown in Fig. 7. Two revolute joints and three rigid bodies are used to better approximate the shape of a deflected beam with an inflection point. The pseudo rigid body model angle, Θ, is taken to be the angle of the beam at the inflection point, θ_i, which is found from the elliptic integral solution.

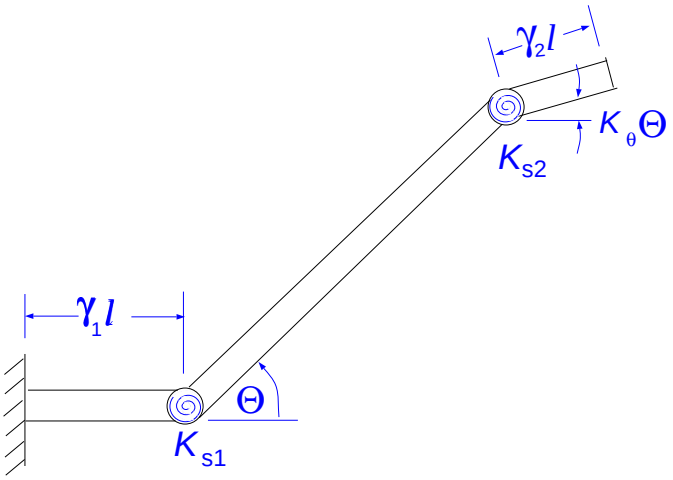

Figure 7. Pseudo rigid body model of a beam with an inflection point.

$$\Theta = \theta_i = \phi - \cos^{-1}\left(\cos(\theta_o - \phi) + \frac{\kappa}{\eta}\right) \tag{31}$$

Using θ_i allows the pseudo rigid body to more closely resemble the deflected beam (increasing accuracy) and avoids problems encountered when trying to determine a pseudo rigid body angle using the position of the beam tip (which can be negative, as seen in Fig. 6). The pivot locations are described by γ_1 and γ_2, as a fraction of the total length of the beam. The angular displacement of the first revolute joint is Θ, and that of the second revolute joint is $K_\theta\Theta$,

where K_θ is the ratio of the angular displacement of the second joint to the first joint. Torsional springs are located at each revolute joint, with stiffness constants K_{s1} and K_{s2}.

For a given κ and η, the range of θ_o which produces an inflection point is determined as described above. Using Eq. (31), the corresponding range of Θ is found. For a pseudo rigid body model with pivot locations and joint displacement ratio γ_1, γ_2, and K_θ, respectively, the position of the output point is

$$\frac{x_p}{l} = \gamma_1 + (1 - \gamma_1 - \gamma_2)\cos\Theta + \gamma_2 \cos K_\theta\Theta \qquad (32)$$

$$\frac{y_p}{l} = (1 - \gamma_1 - \gamma_2)\sin\Theta + \gamma_2 \sin K_\theta\Theta \qquad (33)$$

where (x_p, y_p) is the position of the output point of the pseudo rigid body model. Given κ and η, the range of θ_o and the corresponding range of Θ is divided into N points. For a set of PRBM parameters, the total error is defined as the sum of the squares of the differences between the position of the free end calculated from the elliptic integrals and that obtained from the pseudo rigid body model.

$$e = \frac{1}{l^2}\sum_{i=1}^{N}(x_{oi} - x_{pi})^2 + \left({}^i y_{oi} - {}^i y_{pi}\right)^2 \qquad (34)$$

The optimal values of γ_1, γ_2, and K_θ are ones which minimize this objective function. The PRBM parameters could be determined by directly minimizing Eq. (34); however, this would imply minimization of a function of three variables $(\gamma_1, \gamma_2, K_\theta)$, which could have many local minima. To avoid this, the joint deflection ratio is determined separately from the pivot locations. Since θ_o and $\Theta = \theta_i$ are both given by the elliptic integral solution, a constant relating the two can be found through linear regression. Once K_θ is known, the optimization problem is reduced to two variables (γ_1, γ_2). An ideal model would be accurate for all loading conditions and would be independent of loading conditions. However, the beam tip deflection paths and output angle relationships vary greatly with loading conditions that cause inflection points. Therefore, a model independent of loading conditions will have significant error, whereas a highly accurate model will necessarily vary greatly with loading conditions. So it is desirable to compromise between simplicity and accuracy. If γ_1 and γ_2 are independent, there are large variations for high values of η. Therefore, a predetermined relationship is set between the pivot locations, such as $\gamma_1 = c\gamma_2$, where c is a constant.

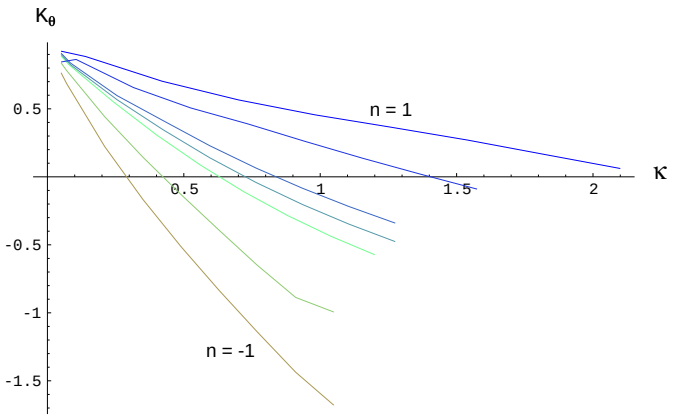

Figure 8. Ratio of joint deflections as a function of loading conditions.

Various values of c were tried, and it was found that $c = 1$ decreased the variation in pivot locations without increasing the error drastically. In this way, the optimization problem is reduced to minimization of a function of one variable.

PIVOT LOCATIONS AND JOINT DEFLECTION RATIOS

As discussed previously, there is a finite range of θ_o over which an inflection point exists, which varies with κ and n. For values of n between -1 and 1, the range of θ_o is greater than 20°, some of which is in the range $-45° \le \theta_o \le 45°$. However for $n > 1$, no inflection point exists with a θ_o less than 45°. For $n < -1$, the range of θ_o becomes very small (in most cases, about 1°). In these cases, the range of output positions and α is correspondingly small. So for $n < -1$, almost all values of α will not produce an inflection point, and an inflection point will only occur for α very close to the maximum permissible value. Therefore, an inflection point model for these values of n is not considered here. For $1 \ge n \ge -1$, the values K_θ and γ obtained from the elliptic integral solution, Eq. (16) - Eq. (18), and the optimization of the error function, Eq. (34), are plotted in Figs. (8) and (9).

From Fig. 8, it is evident that as $\kappa \to 0$, $K_\theta \to 1$ for all values of n. This follows directly from Eq. (31). When $\kappa = 0$, $\Theta = \theta_i = \theta_o$ from (31), and so $K_\theta = 1$. In this case, the model has one pivot point, and from Fig. 9, γ is approximately 0.2, which agrees with existing models for no end moment (Howell, 1995). (Note that previous models have measured pivot locations from the free end to the single pivot, whereas in this case, γ is measured from the fixed end to the single pivot.)

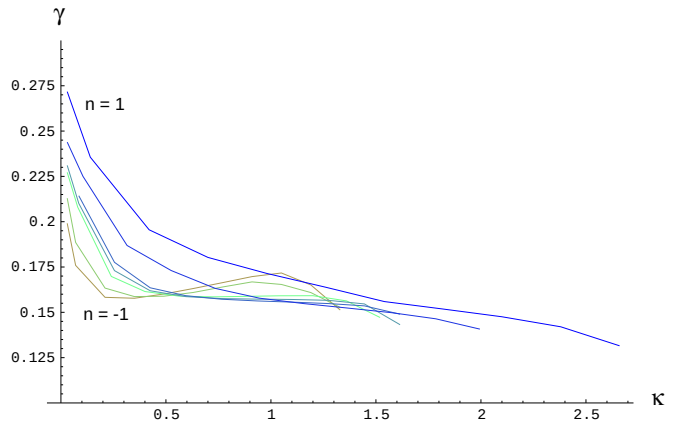

Figure 9. Location of pivot points as a function of loading conditions.

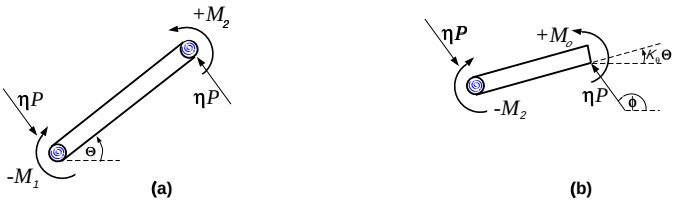

Figure 10. Free body diagrams of the pseudo rigid body model components: (a) the intermediate link with a length of $(1-\gamma_1-\gamma_2)l$, and (b) the output link with a length of $\gamma_2 l$.

DETERMINATION OF SPRING CONSTANTS

The pivot locations and ratio of joint deflections have been determined; now we wish to find the torsional spring constants for each of the pivots. To do so, a moment balance equation is written for the second moving section, which has a length of $\gamma_2 l$ (Fig. 10). The moment at the second joint is denoted M_2.

$$M_2 = P\gamma_2 l\eta \sin(\phi - K_\theta\Theta) + M_o \tag{35}$$

where η and ϕ are defined in Eqs. (21) and (29), respectively. A moment balance equation is also written for the first moving section. The moment at the first joint is denoted M_1.

$$M_1 = P(1-\gamma_1-\gamma_2)l\eta \sin(\phi - \Theta) + M_2 \tag{36}$$

A linear torsional spring is assumed, where the moment produced is directly proportional to the angular deflection with a proportionality constant of K_s. This relationship can be expressed as

$$M_2 = \bar{K}_{s2}(K_\theta - 1)\Theta \tag{37}$$

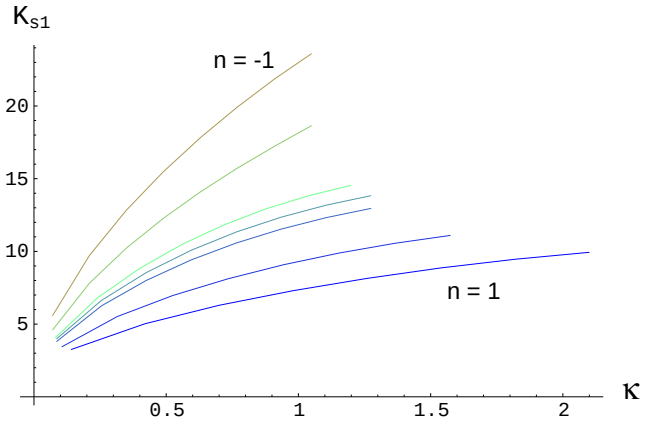

Figure 11. Torsional spring constant of the first pivot as a function of loading conditions.

$$M_1 = \bar{K}_{s1}\Theta \tag{38}$$

where $\bar{K}_s$ has units of moment/radian. Combining Eqs. (35) - (38) to eliminate M_1 and M_2, and multiplying the resulting two equations by l/EI yields

$$K_{s2}(K_\theta - 1)\Theta = \alpha^2\gamma_2\eta\sin(\phi - K_\theta\Theta) - \alpha\sqrt{2\kappa} \tag{39}$$

$$K_{s1}\Theta = \alpha^2(1-\gamma_1-\gamma_2)\eta\sin(\phi-\Theta)+\alpha^2\gamma_2\eta\sin(\phi-K_\theta\Theta)-\alpha\sqrt{2\kappa} \tag{40}$$

where K_s is non-dimensional, and given by the relationship

$$K_s = \bar{K}_s(\frac{l}{EI}). \tag{41}$$

The optimal values of K_{s1} and K_{s2} for a given set of κ and n is found through linear regression by varying the pseudo rigid body angle Θ. The results are shown in Fig. 11 and 12. From Eq. (39), it can be seen that as $K_\theta \to 1$ (which happens when $\kappa \to 0$), the left hand side of Eq. (39) goes to zero, but the right hand does not. Therefore, $K_{s2} \to \infty$. Physically, this can be seen from the fact that as $K_\theta \to 1$, the angular displacement of the second joint goes to zero. But, from the moment balance equation, the moment cannot be zero. Therefore, K_{s2} must approach infinity.

CONCLUSIONS

The fabrication of a 3-D micro-robot, using a two layer SOI wafer bonding process, is presented. The process combines wafer bonding with a series of etching steps to create

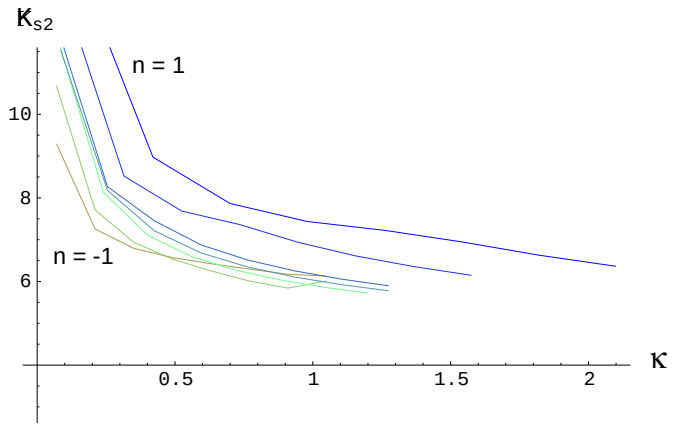

Figure 12. Torsional spring constant of the second pivot as a function of loading conditions.

in-plane and out of plane joints. After the devices are fabricated in a single silicon plane, they can be "popped up" out of the plane for operation. When designing compliant mechanisms, particularly spatial mechanisms such as the one shown here, cases are encountered where moment on the end of the flexural section acts in the opposite direction as the force. Therefore, a model has been developed for such loading conditions. An elliptic integral solution was used to determine the deflection of an individual flexural section and determine when an inflection point would occur. Two joints were used in this model, and first joint angle was taken to be the inflection point angle, allowing the model to closely resemble the actual beam and improving accuracy. The location of the pivot points (measured from each end) varied little and was found to be approximately $0.2l$. The ratio of the joint deflections was found to vary approximately linearly with κ and n. Torsional spring constants were also determined to account for the force and moment required to deflect a compliant mechanism. This model, when combined with existing models, can be used to analyze compliant mechanisms subjected to arbitrary loading conditions, which will be the subject of future study.

ACKNOWLEDGMENTS

This work was supported by DARPA, contract No. DABT 63-98-10015. The support is gratefully acknowledged. The authors would also like to thank Zhongzhou Tang and Zhixiong Liu for their contributions to this work.

REFERENCES

Howell, L. L., 1995, "Parametric Deflection Approximations for End-Loaded, Large Deflection Beams in Compliant Mechanisms," *Journal of Mechanical Design*, Vol. 117, No. 1, pp. 156-165.

Saxena, A. and Kramer, S. N., 1998, "A Simple and Accurate Method for Determining Large Deflections in Compliant Mechanisms Subjected to End Forces and Moments," *Journal of Mechanical Design*, Vol. 120, No. 3, pp. 392-400.

Derderian, J.M., Howell, L.L., et al., 1996, "Compliant Parallel-Guiding Mechanisms," *Proceedings of the 1996 ASME Design Engineering Technical Conferences*, MECH:1208.

Tsai, L.W. and Stamper, R., 1996, "A Parallel Manipulator with only Translational Degrees of Freedom," *Proceedings, 1996 ASME Design Engineering Technical Conferences*, MECH:1152.

Bisshop, K.E., and Drucker, D.C., 1945, "Large Deflection of Cantilever Beams," *Quarterly of Applied Mathematics*, Vol. 3 , No. 3, pp. 272-275.

Frisch-Fay, R., 1963, "Applications of Approximate Expressions for Complete Elliptic Integrals," *International Journal of Mechanical Sciences*, Vol. 5, No. 3, pp. 231-235.

Mattiasson, K., 1981, "Numerical Results from Large Deflection Beam and Frame Problems Analyzed by Means of Elliptic Integrals," *International Journal of Numerical Methods in Engineering*, Vol. 17, pp. 145-153.

Byrd, P.F., and Friedman, M.D., 1954, *Handbook of Elliptic Integrals for Engineers and Physicists*, Springer-Verlag, Berlin.

Midha, A., Norton, T.W., and Howell, L.L., 1994, "On the Nomenclature, Classification, and Abstractions of Compliant Mechanisms," *Journal of Mechanical Design*, Vol. 116, No. 1, pp. 270-279.